PAPER

Study on the regulation of focal adesions and cortical actin by matrix nanotopography in 3D environment

To cite this article: Jingjing Han *et al* 2017 *J. Phys.: Condens. Matter* **29** 455101

View the article online for updates and enhancements.

Study on the regulation of focal adesions and cortical actin by matrix nanotopography in 3D environment

Jingjing Han[1] , **Keng-Hui Lin**[2] **and Lock Yue Chew**[1,3]

[1] School of Physical and Mathematical Sciences, Nanyang Technological University, 21 Nanyang Link, Singapore 637371, Singapore
[2] Institute of Physics, Academia Sinica, Taipei 11529, Taiwan
[3] Complexity Institute, Nanyang Technological University, 18 Nanyang Drive, Singapore 637723, Singapore

E-mail: lockyue@ntu.edu.sg

Abstract

Matrix nanotopography plays an important role in regulating cell behaviors by providing spatial as well as mechanical cues for cells to sense. It has been proposed that nanoscale topography is possible to modulate the tensions which direct the formation of cytoskeleton and the organization of the membrane receptor within the cell, which in turn regulate intracellular mechanical and biochemical signaling. With current studies on this topic being performed mainly in 2D platforms, the question on how nanotopography can influence cell bahaviors in 3D environments has yet to be addressed. In this paper, we explored this question by placing cells in 3D hollow spherical polydimethylsiloxane scaffolds. After culturing rat embryonic fibroblast cells in two kinds of scaffold, one with smooth surface and the other with numerous nano-spikes, we observed that cells in the smooth scaffold have more anchoring sites and more focal adhesions than in the etched scaffold. Moreover, we found the presence of correlation between cortical actin, the important component for supporting cell attachment, and local cell geometry.

S Supplementary material for this article is available online

(Some figures may appear in colour only in the online journal)

1. Introduction

Designing biomaterials, or scaffolds, is a long-standing challenge in the field of tissue engineering and regenerative medicine. Recently increasing attention has been paid to understand the role of the mechanical cues of the scaffolds to cellular behaviors such as differentiation, proliferation, and so on. The mechanical cues include architectural structure of the scaffolds, whose effect on cellular behaviors is multi-scale. At the microscale, it controls cell contact and thus its shape. At the nanoscale it affects cellular receptors due to the size of many cell-signaling molecules [1–3]. The mechanism of how nanotopography affects cellular behaviors is yet to be elucidated. It has been proposed that nanoscale topology likely

modulates the forces which guide cytoskeletal formation and membrane receptor organization in the cell, which in turn can modify intracellular signaling [4, 5]. Most studies on nanotopography were carried out on 2D cultural substrates [6–9]. Only a handful of work studies the nanotopographic effect on cells in 3D [6, 10]. Nevertheless, the 3D matrix structures used in these studies at microscale are quite heterogeneous [11, 12]. The effects of the nanotopography on cells are not at the single cell level [13–15].

In this work, we study the effect of nanotopography on cells at the single cell level by creating a three-dimensional (3D) environment at the micro-scale with different surface roughness at the nano-scale. The 3D microenvironment is a 100 μm spherical pore where two kinds of pore surfaces were
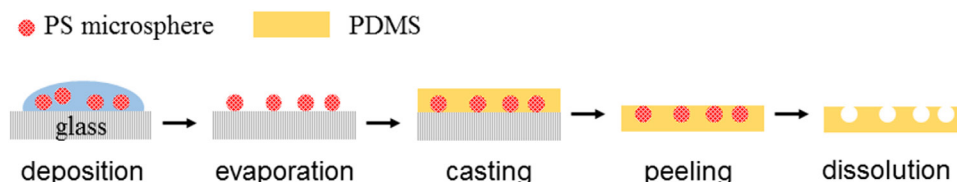
Scheme 1. Schematics for the fabrication of PDMS spherical scaffold with topography cast from that of the polystyrene beads. Polystyrene beads in ethanol were first dropped onto salinized glass slide. After ethanol evaporates, PDMS was poured onto the glass slide. The experimental setup was heated at 80° for 2 h, and the solidified PDMS layer was then peeled off from the glass slide. PDMS was put in DMSO at 140° to dissolve the polystyrene beads to get the PDMS scaffold. In this way, the topography of the microsphere was transferred to the scaffold.

generated. One is smooth and the other is rough with lots of nano-spikes. We compared cell attachments cultured on these smooth and rough surfaces. We found that cells tend to attach its body to the smooth scaffold with more focal adhesions, while cells on the rough surface exhibit less anchoring sites with a reduced number of focal adhesions. Cortical actin is an important component for supporting cell attachments, and it is found to form strong stress fibers frequently in the tube-shaped structure of cell surface. The quantification of cell shape, especially in 3D, is challenging. We adopt the method of a recent work by Elliott *et al* [16], where they compute surface curvature of endothelial cells cultured in 3D collagen matrix. By applying differential geometry and imaging analysis techniques, it is found that when cortical actin intensity increases, the corresponding curvature range becomes smaller. More tube-like structures, which are comprised of strong stress fibers, are found in cells grown in etched scaffold than in unetched scaffold. Moreover, the distribution of surface curvature and actin intensity are different for cells in the two kinds of scaffold due to the effect of attachments and FAs (focal adhesions) distribution. In fact, different parts of the cell surface are observed to exhibit specific range of surface curvature and actin intensity. As a whole, our study shows that in 3D environment, matrix nanotopography influences the formation of focal adhesions, and cortical actin, which is important for supporting cell attachment, is greatly influenced by the local curvature of cell surface.

2. Materials and methods

2.1. Fabricating 3D microenvironment

The 3D microenvironment consists of semi-open spherical pores in polydimethylsiloxane (PDMS) matrix. It is templated by polystyrene microspheres (Polyscience, USA) of diameter 100 μm which are subsequently removed (scheme 1). To create nano-roughened surface, the surface of the polystyrene microspheres were etched by 70% acetone diluted with ethanol for 3 min, followed by rinsing with ethanol for 5 times [17]. We deposited the etched or unetched 0.1 ml polystyrene microspheres suspended in ethanol on a glass slide salinized with 1H,1H,2H,2H-perfluorodecyltrichlorosilane (Alfa Aesar, USA) and baked the solution in the oven for 1 min at 70 °C to evaporate ethanol and leave beads spread on slide. We next

cast mixed PDMS at 10:1 ratio of pre-polymer and curing agent (Sylgard 184, Dow Corning, USA) onto glass slide to form a thin layer. The cast PDMS was cured at 80 °C for 2 h and PDMS film was gently peeled off. The PDMS film was treated in dimethyl sulfoxide (DMSO, J.T.Baker, USA) at 140 °C to dissolve polystyrene microspheres [18] to create hollow spherical pores in PDMS film, which we refer as PDMS scaffolds. The PDMS scaffold was removed from DMSO and heated at 80° for 12 h to remove residual DMSO from PDMS scaffolds. Before seeding the cells, we first treated the PDMS scaffold with oxygen plasma and then incubated PDMS scaffolds in 50 μg ml^{-1} fibronectin (Sigma, USA) with 5 × penicillin (500 μg ml^{-1}) for 2 h at 37° and finally rinsed the scaffolds with phosphate buffered saline (PBS) twice. To visualize the spherical pore, we conjugate cy5 (GE Healthcare) on to fibronectin. For the following discussion, we refer the scaffold made from etched beads as etched scaffold, while the scaffold from unetched beads smooth/unetched scaffold.

2.2. Cell culture and immunostaining

Rat embryonic fibroblast cells stably expressing YFP-Paxillin, which was a generous gift from Dr Cheng-han Yu, were cultured in cell culture dish in Dublecco's Modified Eagle Medium (DMEM) (Life Technologies, USA), supplemented with 10% fetal bovine serum (HyClone, USA) and 1% penicillin streptomysin (Life Technologies, USA). The cells were trypsinized after reaching 80% confluence and a small number of cells were seeded into PDMS spherical scaffold to observe single cell behavior.

Cells were cultured for 5 h for full attachment and then fixed with 4% paraformaldehyde (Sigma, USA) for 10 min, and then permeabilized with 0.5% Triton X-100 for 10 min. Cells were stained with phalloidin-iFluor555 (1:1000 dilution) (AAT Bioquest) for 20 min to visualize F-actin. The samples were embedded in mounting medium made of 60% glycerol, 40% PBS, and 2.3% 1,4-Diazabicyclo[2.2.2]octane for index matching and reducing photobleaching.

2.3. Surface characterization by AFM

The topography of etched and unetched polystyrene microsphere was measured with an atomic force microscope (AFM) (Nanowizard II, JPK, German). 6 μm × 6 μm area of bead top surface was scanned with a silicon cantilever (spring constant:
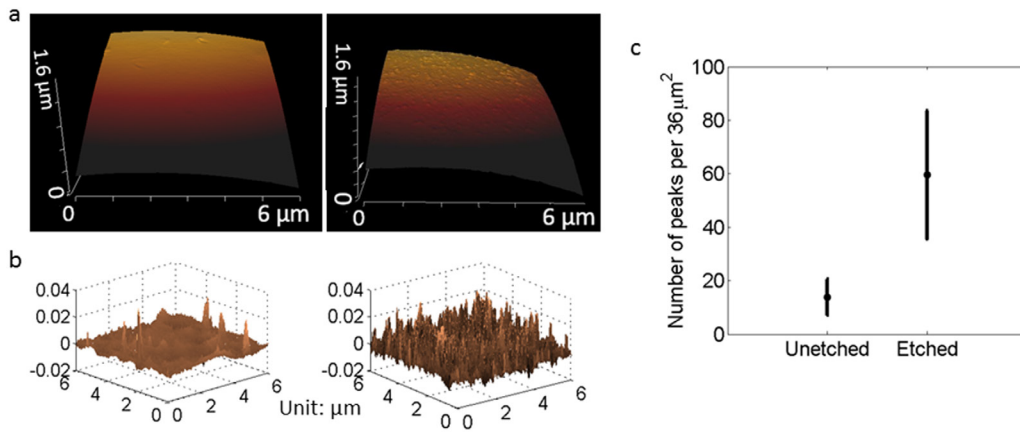
Figure 1. (a) AFM characterization of the topography of polystyrene beads before (left) and after (right) etching by acetone. (b) The topography of unetched beads (left) and etched beads (right) after the removal of surface curvature. (c) Number of peaks per scan area for two groups of beads with $n = 14$ and 11 measurements respectively. Data are shown as mean $\pm$ SD.
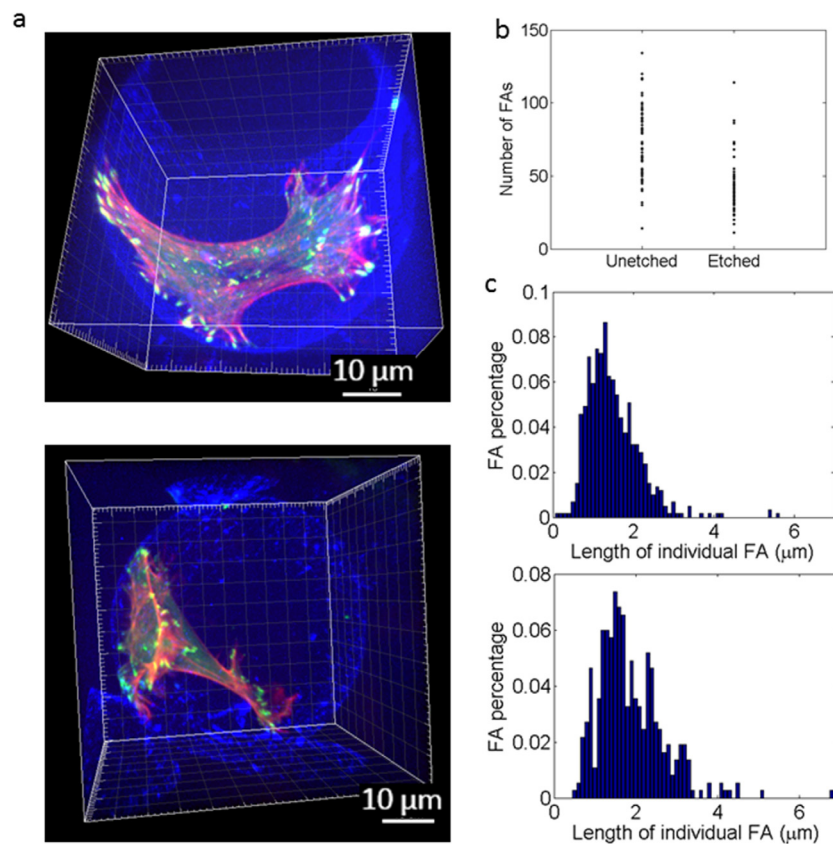

Figure 2. (a) Representative figures of cells expressing YFP-paxillin (green) in unetched (top) and etched (bottom) scaffold. Blue: scaffold, red: actin. (b) Number of focal adhesion streaks per cell. $n = 64$, 60 cells respectively with the use of unpaired student t-test, $p < 0.001$. (c) Normalized individual FA length distribution for cells in unetched (top) and etched (bottom) scaffold group.

$2\,\mathrm{N\,m^{-1}}$) (OMCL-AC240TN-C3, Olympus) in tapping mode. For data analysis, we adopted similar method from [19] to yield the surface curvature. Each individual scan trace was fitted to a circle and then the height due to the arc was subtracted from the original scan. Next we chose 10 nm as the threshold for local peaks and calculated the number of peaks per 6 μm $\times$ 6 μm scan area [20] based on surface topography map after the flattening operations. The significance of the difference in number of local peaks for the two groups of substrate was estimated by the unpaired student t-test.

2.4. Image and analysis

The image stacks were taken with a $63 \times /1.3$ NA glycerol objective on a Leica DMI 6000 microscope with a CSU22 spinning disk confocal unit.

The images were first deconvolved by Huygens 4.5 (scientific volume imaging), and then processed by Imaris 8.1.2. We identified focal adhesion by the built-in surface function with appropriate threshold and then used the bounding box function to measure the focal adhesion length as the maximum
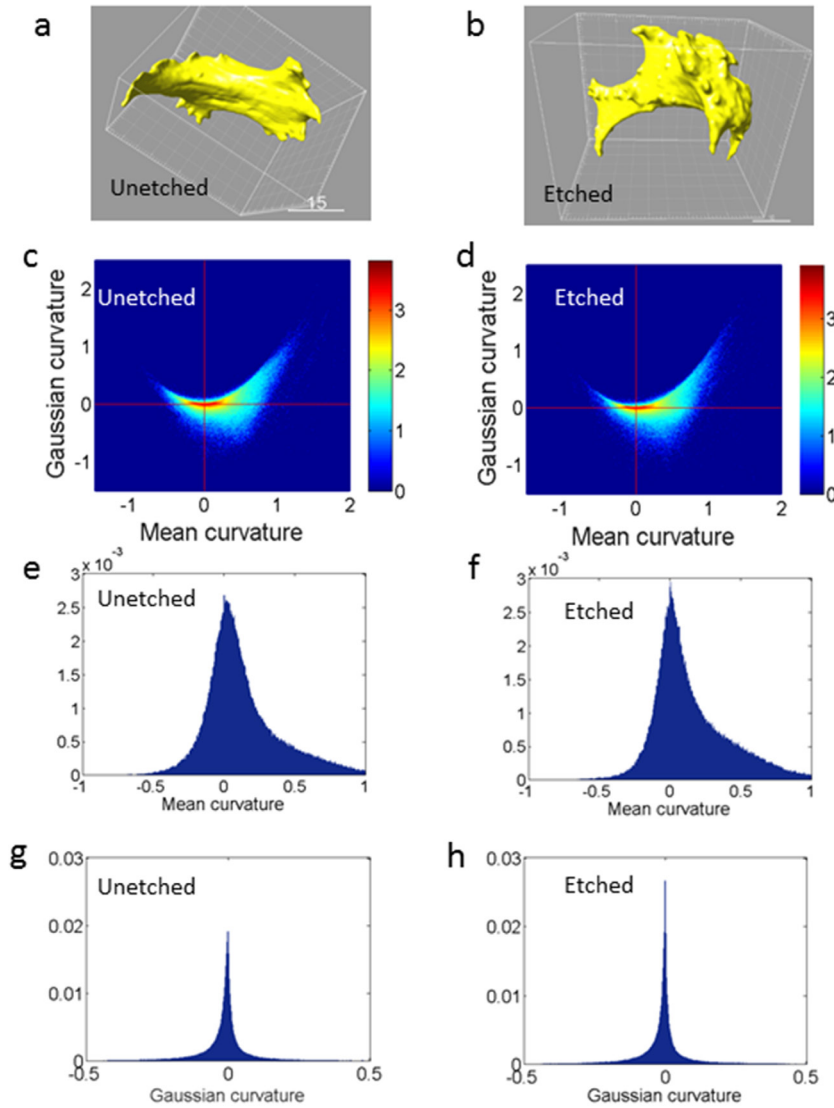
Figure 3. (a) and (b) Representative surface segmentation for cells in unetched (a) and etched (b) assisted by Imaris. (c) and (d) Gaussian curvature versus mean curvature for cells in unetched (c) and etched (d) scaffold. The color indicates log10 of surface points counted. $n = 12$, 12 cells respectively. (e) and (f) Mean curvature normalized distribution for cells in unetched (e) and etched (f) scaffold. Only major range $[-1, 1]$ was shown. $n = 12$, 12 cells respectively. (g) and (h) Gaussian curvature normalized distribution for cells in unetched (g) and etched (h) scaffold. Only major range $[-0.5, 0.5]$ was shown. $n = 12$, 12 cells respectively.

length of the bounding box. Cell surface was segmented from the combined intensity signals of paxillin and F-actin. The combined signal was smoothed by Gaussian filter of kernel size 0.102 μm and then segmented by contour surface function manually (figures 3(a) and (b)). The cell surface was represented by a triangulated-mesh and exported to MATLAB for later analysis. The local surface curvature of cell surface was calculated based on the algorithm from [21]. Throughout our study, we used locally averaged curvature, which is the mean value of all curvature within a sampling sphere of radius 1 μm [16]. The same sampling scale was also applied to the calculation of the intensity value of actin cortex as the average value of all vertices falling within the sampling sphere (S1(a)). Note that actin intensity was normalized using the method proposed in [16].

In order to study the role of different parts of the cell surface in regulating cell morphology, we split the cell surface into three parts and investigated them separately. First, the 3D

cell object was rotated along the *x* and *y* axis at various angles to obtain the maximum 2D projection onto the *xy* plane, which gives our cell boundary in 2D. Next, by taking the *x*, *y* coordinates of all vertices and considering all the vertices which are at a distance of 1–1.5 μm from the 2D boundary in *xy* plane, we form the cell boundary in 3D which also includes the 2D cell boundary. After removing this defined 3D cell boundary from the cell surface, two major clusters of vertices remain. They are split into the basal part which got attached to the scaffold, and the apical part which is located away from the scaffold.

3. Results and discussions

As it is difficult to measure the topography of the surface of the pore, our measurement of the nano-topography is based on the template particles (figure 1(a)). With PDMS being used for
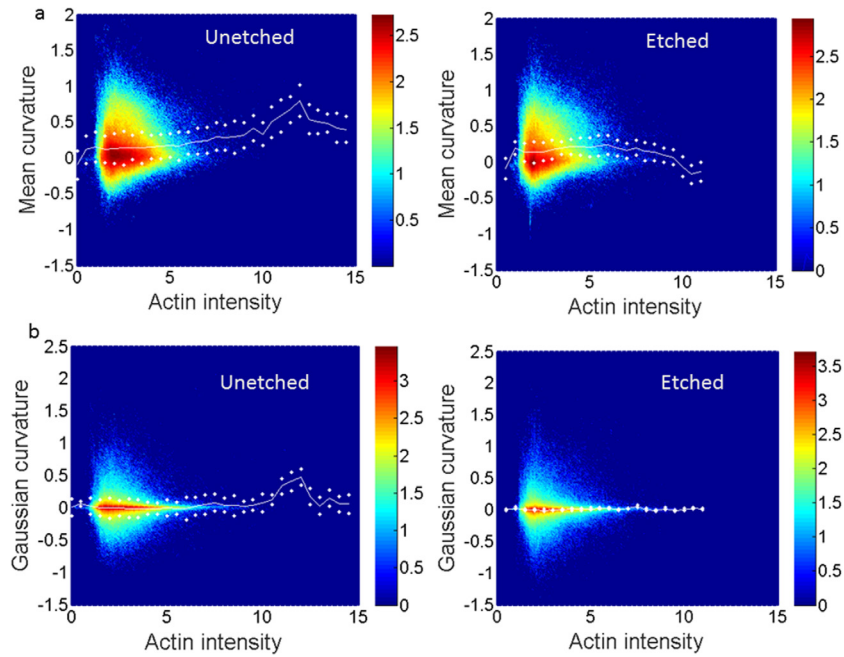
Figure 4. (a) Cortical actin intensity versus mean curvature for cells in unetched (left) and etched (right) scaffold. The color indicates log10 of the number of data points. $n = 12$, 12 cells respectively. (b) Cortical actin intensity versus Gaussian curvature for cells in unetched (left) and etched (right) scaffold. Solid line is the mean value for each intensity value, and dashed line is bootstrapped 95% confidence intervals of the mean. The color indicates log10 of the number of data points. $n = 12$, 12 cells respectively.
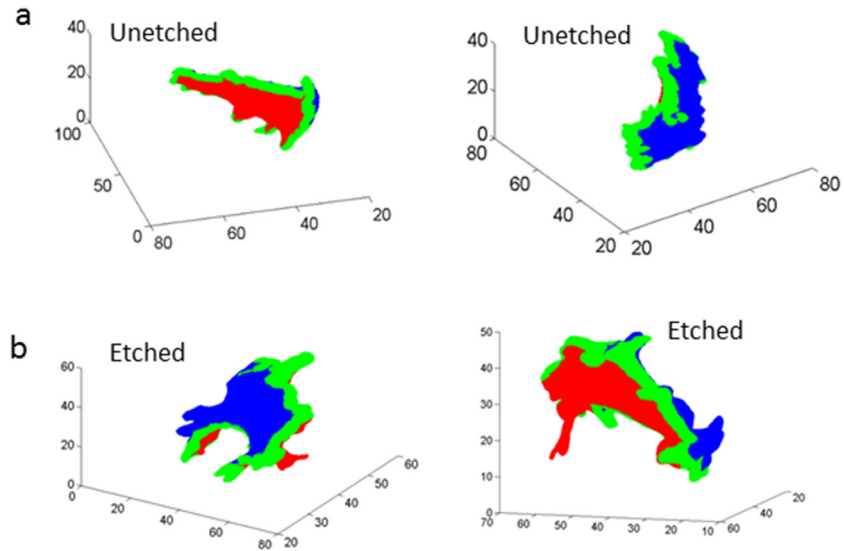

Figure 5. Representative figure of cell surface split into boundary (green), basal (blue), and apical (red) part for unetched group (panel (a)) and etched group (panel (b)).

nano-imprint (reference), we believe that the nano-features created on the template particles are preserved in the PDMS scaffolds. After flattening operations with AFM measurement that excludes the effect of surface curvature (figure 1(b)), local spikes higher than 10 nm are defined as peaks, which is a commonly defined spacing parameter [20]. The AFM results showed that there are around 60 nanospikes on $6 * 6 \ \mu m^2$ scanning area of etched microsphere, while there are only 15 nanospikes for that of unetched microsphere (figure 1(c)).

We observed that cells exhibit distinctive attachments on the two scaffolds. In the smooth scaffold, cells tend to have more attachments to the inner surface of the scaffold than cells

in the etched scaffold (figure 2(a)). We found that there are more focal adhesions for cells on smooth scaffolds than cells on rough scaffolds (figure 2(b)), which might arise from more cell attachments to the scaffold in the former than in the latter case. In 2D, a positive correlation between cell area and total focal adhesion size was reported [22], and less focal adhesions were found for cells on micro-rough surface compared to that on smooth surface [23]. Moreover, cell adhesion was reported to be larger on rough substrate in 2D study [24, 25]. Thus we speculate that the stronger adhesion on etched scaffold implies that a small attachment area is sufficient for the cell. However, there is little difference in focal adhesion size for cells on both
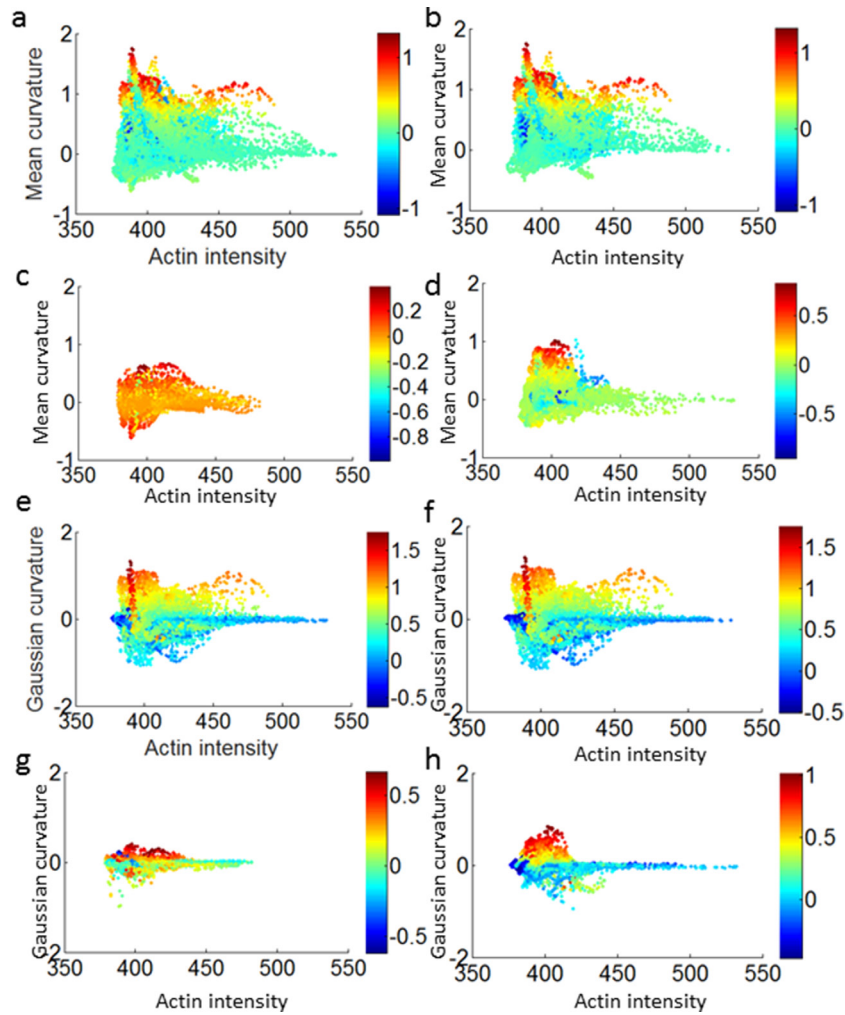
Figure 6. Cortical actin intensity versus mean curvature for cell whole surface (a), boundary (b), apical (c), and basal (d) part of one representative cell from unetched group. Cortical actin intensity versus Gaussian curvature for cell whole surface (e), boundary (f), apical (g), and basal (h) part of the same cell. The scale bar indicates the value of curvature.

surfaces. The focal adhesion size range from 0.5 μm to 3 μm (figure 2(c)) and is generally smaller than focal adhesion on 2D substrates. It is surprising that the nanotopography of the scaffold does not affect the focal adhesion size.

As we observed stress fibers more likely to appear in tube-shaped structure of cell surface, we speculate this might be related with surface local geometry. To quantify cell surface further, we computed the local mean and Gaussian curvature (S1(b) and (c)) for cell surface segmented from Imaris (figures 3(a) and (b)). For the whole study to be consistent, surface curvature and actin intensity in later results are used after spherical sampling with radius of 1 μm (materials and methods). The plot of mean curvature against Gaussian curvature shows that most of the value of curvature falls around region where Gaussian curvature is close to zero with mean curvature in the range of -0.3 to 0.3 for both group of cells. Furthermore, the least number of data points falls in the 2nd quadrant (figures 3(c) and (d)), which corresponds to an invagination-shaped structure [16]. These results indicate that the local curvature of cell surface is not random but are limited to a certain range such that extremely large curvature rarely exists. Similar findings were also reported in primary

aortic endothelial cells embedded in collagen gels [16]. In particular, the peaks around zero for both histograms of mean and Gaussian curvature are found to be higher and narrower for those in the etched group than those in the unetched group (figures 3(e)–(h)). This is further affirmed by the full width Half maximum (FWHM) of the mean curvature distribution plot which gives a value of 0.2092 for the etched group and 0.2536 for the unetched group. Similarly, the FWHM of Gaussian curvature distribution plot is 0.0122 for the etched group and 0.0217 for the unetched group. Besides, bootstrap method is applied to get the 95% confidence intervals (use 'deviation' to indicate here) of the mean of mean/Gaussian curvature at each actin intensity. The deviations are smaller in etched group that the average deviation of mean curvature in unetched group is 0.1928, and 0.1163 in etched group; the average deviation of Gaussian curvature in unetched group is 0.1210, and 0.0150 in etched group. Next student *t*-test was applied to test the statistical significance of deviation. The results show that the deviation for Gaussian curvature distribution in unetched and etched case is statistically significant with p value smaller than 0.001, and the mean curvature distribution in unetched and etched case is also statistically
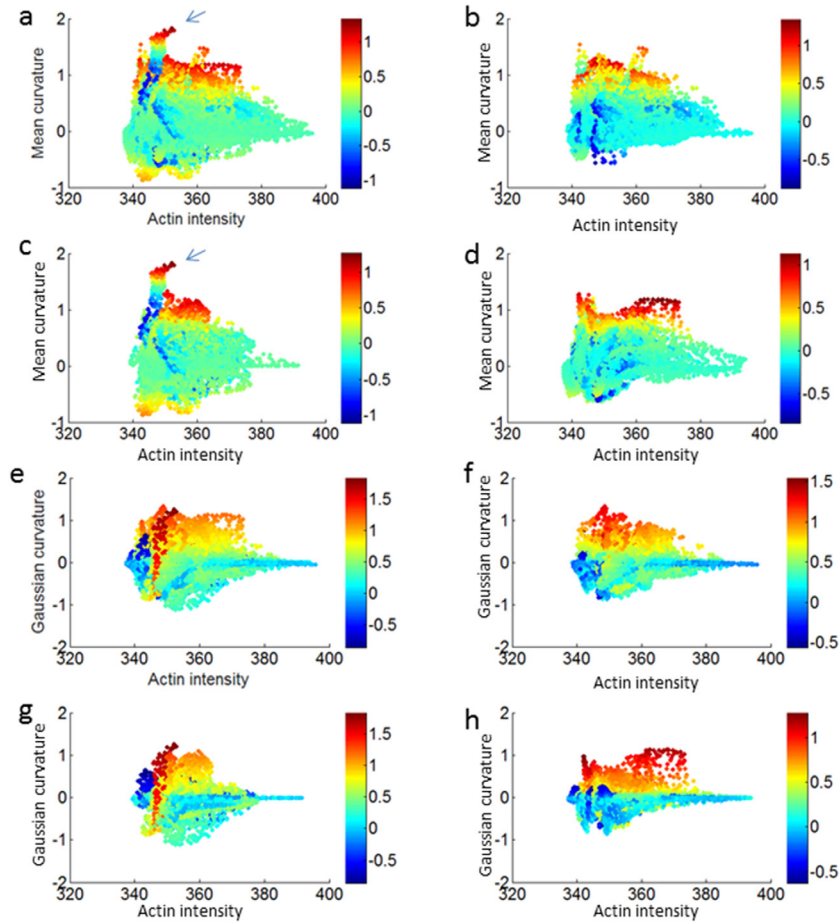
Figure 7. Cortical actin intensity versus mean curvature for cell whole surface (a), boundary (b), apical (c), and basal (d) part of one representative cell from etched group. Cortical actin intensity versus Gaussian curvature for cell whole surface (e), boundary (f), apical (g), and basal (h) part of the same cell. The scale bar indicates the value of curvature.

significant with p value smaller than 0.001. This is consistent with a smaller FWMH in etched group, suggesting a more concentrated curvature distribution. The Gaussian distribution being relatively more concentrated around 0 suggests that there are more tube-shaped structures formed on the cell surface for cells cultured on etched scaffold, which might arise from fewer anchoring sites.

Next, we noticed that actin stress fibers appear mostly in regions where the cell body is elongated (S2) and rarely in places where the cell surface is highly curved. This suggests that actin distribution (S1(a)) might be linked to local cell surface curvature. This leads us to investigate the correlation between cortical actin intensity and local mean curvature/Gaussian curvature (figures 4(a) and (b)). The plots of normalized actin intensity against mean curvature show that for either cell in unetched or etched scaffold, when cortical actin intensity increases, the corresponding curvature range becomes smaller. Most importantly, this correlation is consistent with experimental findings that strong stress fibers mostly appear at region where Gaussian curvature is close to zero, which corresponds to tube-like structure [16]. In fact, stress fibers are observed to appear mostly at tube shaped area on cell surface and this applies to 2D study on stress fibers as well. Moreover, the major actin intensity and mean/Gaussian curvature distribution for cells in etched scaffold are found to concentrate within a small range, compared to the relatively large variation for cells in unetched scaffold. The decrease of focal adhesions for cells in etched scaffold may cause a decrease in ways for actin to be distributed or aligned, which results in a smaller actin intensity range. Moreover, there are strong interactions between FAs and actin via the many actin-binding proteins. The regulation of actin dynamics has also been associated with FAs [26], while actin is known to influence the stability of FAs [27, 28]. In fact, we observe that most focal adhesions appear mainly at the two ends of the actin filaments. In 2D, a strong correlation between focal adhesion complex and F-actin fiber alignment was reported. A decrease in FA area is found to favor higher F-actin alignment [29], which is consistent with our study that highly aligned stress fibers are more likely to occur for cells in etched scaffold with less focal adhesions compared to cells in smooth scaffold with more focal adhesions.

After obtaining the correlation between cortical actin intensity and cell surface curvature for the whole cell, it remains to determine the different roles play by different parts of the cell surface in actin intensity and surface curvature regulation, and it's possible that different segments of cell body have their own specific distributions of cortical actin and curvature. The past study has shown that different parts of cell may exhibit their own specific behaviors. For example, the traction force

distribution inside a cell is not homogeneous, and most of the forces are concentrated in cell border while only a very small percentage of forces are concentrated in the middle of cell. In our study, the most distal contacts made by the cell with the spherical scaffold is critical to define the cell shape in 3D, and cortical actin is the important component for maintaining cell shape. First, we obtain the maximum 2D projection of the 3D cell morphology. We then define the projection boundary together with all the neighboring points as the boundary in 3D (materials and methods). Next, the cell surface except the cell boundary is divided into the 'apical' and 'basal' parts depending on whether they get attached to the matrix or they are away from matrix (figure 5). We could see the cell boundary is crucial to determine the cell shape (figure 5) and it connects the cell 'basal' (closer to the substrate) and 'apical' (away from the substrate) parts, and as the bridge between 'basal' and 'apical', it also contains many high curvature structures.

After segmenting the cell surface into three parts: boundary, apical, and basal, we studied the correlation between actin intensity and surface curvature for each part in unetched (figure 6) and etched group (figure 7) respectively.

Interestingly, the distribution of actin intensity with mean curvature (figures 6(a)–(d) and 7(a)–(d)) and Gaussian curvature (figures 6(e)–(h) and 7(e)–(h)) exhibits similar pattern for the whole cell and the cell boundary. This indicates that cell boundary is critical to determine the cell shape. The high curvature is likely to happen in boundary part (figure 6(b)), while it is also possible for the tiny structures, like some local bumps, on basal or apical surface to possess high curvature, as the arrow indicated (figures 7(a) and (c)). Highest actin intensity is frequently found to appear at the region where cell adheres to the scaffold. For cells in unetched scaffold, it is more likely to happen in basal part, due to the great attachments. While, if most of the adhesions come from the attach of boundary part to scaffold, which is more likely to happen in cells of etched group, the highest actin may also arise from the boundary region (figure 7(b)). Another impact factor is the formation of stress fibers, which has been observed to have a preference towards cell boundary (figure 2(a)) and is also of great intensity. Through our investigation, in terms of different subunits, we have observed that each part of the cell surface plays independent while interconnected role in regulating surface curvature as well as cortical actin distribution.

5. Conclusions

In conclusion, we carried out a highly effective method of fabricating 3D spherical pore scaffold with controlled nanotopography and conducted the study on the influence of matrix topography on cell behaviors in 3D. The cells are observed to exhibit dissimilar attachments and different number of focal adhesions in two kinds of scaffold: unetched scaffold and etched scaffold with nano-spikes. Our results show the presence of a correlation between cortical actin, the important component for supporting cell attachment, and local cell geometry, which implies the influence of 3D matrix topography on cell bahaviors through the regulation of actin and focal adhesion distribution. It highlights the potential of applying 3D matrix topography to manipulate cell behavior for the design of biomedical devices.

Author contributions

JJH and KHL designed the experiment. JJH conducted the experiment. JJH, KHL, and LYC did the data analysis. JJH, KHL, and LYC wrote the manuscript. The manuscript was written through contributions of all authors. All authors have given approval to the final version of the manuscript.

Conflicts of interest

The authors declare no conflict of interest.

Supplementary materials

Supplementary materials can be found at the other.doc file: 'supporting information for Publication.pdf' (stacks.iop.org/JPhysCM/29/455101/mmedia).

ORCID iDs

Jingjing Han ⬤ https://orcid.org/0000-0002-9663-0263

References

[1] Dalby M J, Gadegaard N and Oreffo R O C 2014 Harnessing nanotopography and integrin-matrix interactions to influence stem cell fate *Nat. Mater.* **13** 558–69
[2] Antoni D, Burckel H, Josset E and Noel G 2015 Three-dimensional cell culture: a breakthrough *in vivo Int. J. Mol. Sci.* **16** 5517–27
[3] Lee J, Cuddihy M J and Kotov N A 2008 Three-dimensional cell culture matrices: state of the art *Tissue Eng.* B **14** 61–86
[4] Stevens M M and George J H 2005 Exploring and engineering the cell surface interface *Science* **310** 1135–8
[5] Andersson A-S, Brink J, Lidberg U and Sutherland D S 2003 Influence of systematically varied nanoscale topography on the morphology of epithelial cells *IEEE Trans. Nanobiosci.* **2** 49–57
[6] Kim D-H, Provenzano P P, Smith C L and Levchenko A 2012 Matrix nanotopography as a regulator of cell function *J. Cell Biol.* **197** 351–60

[7] Bettinger C J, Langer R and Borenstein J T 2009 Engineering substrate topography at the micro-and nanoscale to control cell function *Angew. Chem., Int. Ed.* **48** 5406–15

[8] Baik K Y, Park S Y, Namgung S, Kim D, Cho D-G, Lee M and Hong S 2014 Synthetic nanowire/nanotube-based solid substrates for controlled cell growth *Nano Converg.* **1** 1

[9] Janson I A, Kong Y P and Putnam A J 2014 Nanotopographic substrates of poly (methyl methacrylate) do not strongly influence the osteogenic phenotype of mesenchymal stem cells in vitro *PloS One* **9** e90719

[10] Choi C-H, Hagvall S H, Wu B M, Dunn J C and Beygui R E 2007 Cell interaction with three-dimensional sharp-tip nanotopography *Biomaterials* **28** 1672–9

[11] Härmä V, Schukov H-P, Happonen A, Ahonen I, Virtanen J, Siitari H, Åkerfelt M, Lötjönen J and Nees M 2014 Quantification of dynamic morphological drug responses in 3D organotypic cell cultures by automated image analysis *PloS One* **9** e96426

[12] Zaman M H, Trapani L M, Sieminski A L, MacKellar D, Gong H, Kamm R D, Wells A, Lauffenburger D A and Matsudaira P 2006 Migration of tumor cells in 3D matrices is governed by matrix stiffness along with cell-matrix adhesion and proteolysis *Proc. Natl Acad. Sci.* **103** 10889–94

[13] Mendes P M 2013 Cellular nanotechnology: making biological interfaces smarter *Chem. Soc. Rev.* **42** 9207–18

[14] Salmasi S, Kalaskar D M, Yoon W-W, Blunn G W and Seifalian A M 2015 Role of nanotopography in the development of tissue engineered 3D organs and tissues using mesenchymal stem cells *World J. Stem Cells* **7** 266

[15] Kshitiz X, Afzal J, Kim S-Y and Kim D-H A 2014 Nanotopography approach for studying the structure-function relationships of cells and tissues *Cell Adhes. Migr.* **9** 300–7

[16] Elliott H, Fischer R S, Myers K A, Desai R A, Gao L, Chen C S, Adelstein R S, Waterman C M and Danuser G 2015 Myosin II controls cellular branching morphogenesis and migration in three dimensions by minimizing cell-surface curvature *Nat. Cell Biol.* **17** 137

[17] Han J, Menon N V, Kang Y and Tee S-Y 2015 An *in vitro* study on the collective tumor cell migration on nanoroughened poly (dimethylsiloxane) surfaces *J. Mater. Chem.* B **3** 1565–72

[18] Subramaniam A B, Lecuyer S, Ramamurthi K S, Losick R and Stone H A 2010 Particle/fluid interface replication as a means of producing topographically patterned polydimethylsiloxane surfaces for deposition of lipid bilayers *Adv. Mater.* **22** 2142–7

[19] Shellenberger K and Logan B E 2002 Effect of molecular scale roughness of glass beads on colloidal and bacterial deposition *Environ. Sci. Technol.* **36** 184–9

[20] Raposo M, Ferreira Q and Ribeiro P 2007 A guide for atomic force microscopy analysis of soft-condensed matter *Mod. Res. Educ. Top. Microsc.* **1** 758–69

[21] Theisel H, Rossi C, Zayer R and Seidel H-P 2004 Normal based estimation of the curvature tensor for triangular meshes *12th Pacific Conf. on Computer Graphics and Applications PG 2004 (IEEE)* pp 288–97

[22] Chen C S, Alonso J L, Ostuni E, Whitesides G M and Ingber D E 2003 Cell shape provides global control of focal adhesion assembly *Biochem. Biophys. Res. Commun.* **307** 355–61

[23] Diener A, Nebe B, Lüthen F, Becker P, Beck U, Neumann H G and Rychly J 2005 Control of focal adhesion dynamics by material surface characteristics *Biomaterials* **26** 383–92

[24] Chen W, Villa-Diaz L G, Sun Y, Weng S, Kim J K, Lam R H, Han L, Fan R, Krebsbach P H and Fu J 2012 Nanotopography influences adhesion, spreading, and self-renewal of human embryonic stem cells *ACS Nano* **6** 4094–103

[25] Dowling D P, Miller I S, Ardhaoui M and Gallagher W M 2011 Effect of surface wettability and topography on the adhesion of osteosarcoma cells on plasma-modified polystyrene *J. Biomater. Appl.* **26** 327–47

[26] Le Clainche C and Carlier M-F 2008 Regulation of actin assembly associated with protrusion and adhesion in cell migration *Physiol. Rev.* **88** 489–513

[27] Wehrle-Haller B 2012 Assembly and disassembly of cell matrix adhesions *Curr. Opin. Cell Biol.* **24** 569–81

[28] Kaverina I, Krylyshkina O and Small J V 2002 Regulation of substrate adhesion dynamics during cell motility *Int. J. Biochem. Cell Biol.* **34** 746–61

[29] Lipski A M, Pino C J, Haselton F R, Chen I-W and Shastri V P 2008 The effect of silica nanoparticle-modified surfaces on cell morphology, cytoskeletal organization and function *Biomaterials* **29** 3836–46